



**HAL**  
open science

## Per-pixel unmixing of spectrally overlapping fluorophores using intra-exposure excitation modulation.

H. Valenta, F. Bierbuesse, Raffaele Vitale, Cyril Ruckebusch, W. Vandenberg, P. Dedecker

### ► To cite this version:

H. Valenta, F. Bierbuesse, Raffaele Vitale, Cyril Ruckebusch, W. Vandenberg, et al.. Per-pixel unmixing of spectrally overlapping fluorophores using intra-exposure excitation modulation.. Talanta, 2023, Talanta, 269, pp.125397. 10.1016/j.talanta.2023.125397 . hal-04500061

**HAL Id: hal-04500061**

**<https://hal.univ-lille.fr/hal-04500061v1>**

Submitted on 11 Mar 2024

**HAL** is a multi-disciplinary open access archive for the deposit and dissemination of scientific research documents, whether they are published or not. The documents may come from teaching and research institutions in France or abroad, or from public or private research centers.

L'archive ouverte pluridisciplinaire **HAL**, est destinée au dépôt et à la diffusion de documents scientifiques de niveau recherche, publiés ou non, émanant des établissements d'enseignement et de recherche français ou étrangers, des laboratoires publics ou privés.



Distributed under a Creative Commons Attribution 4.0 International License



# Per-pixel unmixing of spectrally overlapping fluorophores using intra-exposure excitation modulation

Hana Valenta<sup>a,1</sup>, Franziska Bierbuesse<sup>a,1</sup>, Raffaele Vitale<sup>b</sup>, Cyril Ruckebusch<sup>b</sup>, Wim Vandenberg<sup>a</sup>, Peter Dedecker<sup>a,\*</sup>

<sup>a</sup> Department of Chemistry, KU Leuven, Belgium

<sup>b</sup> U. Lille, CNRS, LASIRE, France

## ARTICLE INFO

Handling Editor: Prof A Campiglia

### Keywords:

Multiplexed imaging  
Per-pixel unmixing  
Reversibly photoswitchable fluorescent proteins

## ABSTRACT

Multilabel fluorescence imaging is essential for the visualization of complex systems, though a major challenge is the limited width of the useable spectral window. Here, we present a new method, exNEEMO, that enables per-pixel quantification of spectrally-overlapping fluorophores based on their light-induced dynamics, in a way that is compatible with a very broad range of timescales over which these dynamics may occur. Our approach makes use of intra-exposure modulation of the excitation light to distinguish the different emitters given their reference responses to this modulation. We use the approach to simultaneously image four green photochromic fluorescent proteins at the full spatial resolution of the imaging.

## 1. Introduction

Fluorescence microscopy is a key technology in life sciences, though it is limited in the number of components that can be visualized at once. Several solutions to address this limitation have been developed, including computational approaches based on spectral unmixing [1] or the use of fluorescence properties other than the emission color, such as fluorescence anisotropy [2], fluorescence lifetime [3], or light-induced processes resulting in characteristic fluorescence dynamics in the emission [4–7].

We recently developed emitter separation based on intra-exposure excitation modulation [8], a method that can distinguish multiple spectrally-identical fluorophores based on differences in their light-induced fluorescence dynamics that can occur over a broad range of timescales. Using this approach, which we retroactively named intra-exposure excitation modulation (NEEMO), we were able to distinguish the light-induced dynamics of four spectrally-identical reversibly photoswitchable fluorescent proteins (rsFPs) expressed within *E. coli* bacteria. Such labels can be controllably switched between a fluorescent and a nonfluorescent state using illumination at two different wavelengths.

This previous work focused on the classification of cells expressing just one of these fluorophores rather than on the separation of the

fluorophore contributions within potentially complex mixtures. Classifications are easier to achieve since the signal can be averaged over the entire cell geometry, leading to much better signal-to-noise ratios, while the analysis can be based on clustering approaches that are tolerant to changes in label behavior as long as each cell can still be assigned to the correct cluster. Such an approach has also been used to, for example, distinguish up to 9 among 16 spectrally similar fluorophores expressed in bacteria [9].

The true quantitative separation of fluorophores based on their fluorescence dynamics has also seen multiple efforts over the past years, resulting in approaches such as OLID, SAFIRE, OPIOM, and HIGHLIGHT [9–14], that make use of the direct detection of the fluorescence dynamics by the microscope. This may, however, be challenging if the detection is done using a camera that is typically much slower than the point detectors used in confocal imaging, meaning that only correspondingly slow fluorescence dynamics can be used.

In this manuscript, we explored whether our previous concept can be extended to provide a quantitative emitter separation in complex mixtures, in a manner that takes advantage of the full spatial resolution of the imaging while still being capable of leveraging fluorescence dynamics that occur too quickly to be captured by the detector. In particular, we present the extended intra-exposure excitation modulation (exNEEMO) method that permits the per-pixel separation of four

\* Corresponding author.

E-mail address: [peter.dedecker@kuleuven.be](mailto:peter.dedecker@kuleuven.be) (P. Dedecker).

<sup>1</sup> These authors contributed equally to this work.

spectrally-identical rsFPs based on their unique photoswitching profiles, using the acquisition of just four fluorescence images. We find that this can be successfully achieved while retaining compatibility with a broad range of light-induced fluorescence dynamics, though the overall accuracy is limited by cell-to-cell variations in these dynamics. Overall, our approach enables new dimensions for the multiplexed fluorescence imaging of complex biological systems.

## 2. Results and discussion

We start by briefly revisiting the principle underlying the NEEMO method, schematically shown in Fig. 1A and previously reported in Ref. [8]. The core idea is that different photoswitching efficiencies of the fluorophores lead to characteristic emission intensity profiles in response to temporally-varying illumination intensities. In NEEMO, we do not detect these responses directly, but instead measure only their integrated emission over the camera exposure time. The different labels can then be identified by observing how the integrated intensities vary for different illumination patterns [8]. This approach is compatible with a very broad range of processes since we do not require that the dynamics are directly resolvable by the imaging system. Instead, we require only that they can be probed within the modulation rate of the light sources, which is typically very fast (within microseconds or faster) even for inexpensive light sources.

In our previous study, the acquisition of two to four fluorescence images with different excitation light modulations was sufficient to classify four different types of fluorophores according to their photoswitching efficiencies. To test this approach in complex mixtures, we expressed the same fluorophores in HeLa cells using different targeting motifs for each label. In particular, we targeted EGFP to the plasma membrane using the Lyn targeting motif (Lyn-EGFP), ffDronpa to the nucleus via fusion with histone-H2B (H2B-ffDronpa), ffDronpaF to vimentin-based fibres via fusion to vimentin (vimentin-ffDronpaF), ffDronpa2F to peroxisomes (peroxisome-ffDronpa2F), each showing very different switching responses (Supplementary Fig. S1). To quantitatively separate mixtures of these fluorophores, the number of acquired images must at least be equal to the number of components in the mixture, and hence we exposed each of these fluorophores to four different illumination modulations (see Fig. 1B). The resulting acquisitions revealed both the expected cellular localizations of the labels as well as the pronounced differences in their responses to the illumination (see Fig. 1C and Supplementary Movies S1-4). We then repeated this procedure over many cells expressing single constructs, allowing the measurement of the fluorescence reference profiles for the expressed fluorophore (see Fig. 1D). These profiles encode the characteristic response of each type of fluorophore to the illumination modulation.

The characteristic fluorophore responses were apparent also when imaging HeLa cells expressing all four labels simultaneously (see Fig. 2A and Supplementary Movie S5), though it is difficult to distinguish the four rsFPs in the measured images by eye due to their strong spatial overlap within the cell. We instead analyzed these images using non-negative least squares [15]. In this approach, the measured image ( $\mathbf{X}$ ) is decomposed into the product of the local abundances of each fluorophore ( $\mathbf{A}$ ) and the known responses of these fluorophores to the illumination modulation obtained via the single-label experiments ( $\mathbf{S}$ ) under a non-negativity constraint [16,17].

Because the measurement is susceptible to noise, we must also include an error term  $\mathbf{E}$  such that

$$\mathbf{X} = \mathbf{A}\mathbf{S}^T + \mathbf{E} \quad (1)$$

Given  $\mathbf{X}$  and  $\mathbf{S}$ , the least-squares analysis sets out to solve this system of equations in order to determine  $\mathbf{A}$ .

In our experiments,  $\mathbf{X}$ ,  $\mathbf{A}$ , and  $\mathbf{E}$  are of dimensions  $N \times 4$ , where  $N$  is the total number of non-background pixels in a fluorescence image and 4 is the number of acquired images. To fill  $\mathbf{X}$ , the four images acquired

with different illumination patterns are simply unfolded by concatenating all of the pixel values from a given image into the individual columns of  $\mathbf{X}$ . The matrix  $\mathbf{S}$  is a  $4 \times 4$  matrix containing the responses of the fluorophores as determined from the single-fluorophore control measurements. The dimensions of this matrix arise because we have four different fluorophores and four different modulation patterns (fluorescence images). More information on the analysis is provided in the Methods section of this work.

Fig. 2B shows an example result from this analysis, showing that the contributions of the different fluorophores can be selectively extracted to reveal their expected intracellular targeting. Fig. 2C displays each of the calculated fluorophore distributions in separate image plots, making it possible to observe whether there is crosstalk between the different channels. The different fluorophore distributions are readily distinguishable, though some crosstalk is observed between the EGFP and ffDronpa signals. This crosstalk reflects the closer correspondence between the responses of these fluorophores to the illumination modulations (Fig. 1D). Supplementary Fig. S2 shows additional results of the exNEEMO procedure obtained on randomly-selected cells expressing these constructs.

The exNEEMO analysis decomposes the acquired fluorescence images using the provided single-fluorophore reference profiles, by determining the weighted sum of the reference profiles that best describes the experimental data acquired in each pixel. Scaling the values of a reference profile by a factor  $B$  therefore results in a rescaling of the calculated fluorophore abundance by a factor  $1/B$ . However, regardless of any such scaling, the obtained fluorophore abundances will be proportional to the local fluorophore concentrations, which is exactly the assumption that is applied in the vast majority of fluorescence imaging experiments. The results of our method are therefore compatible with a variety of downstream analysis pipelines and approaches. However, because it relies on the absolute quantification of the emitted fluorescence, the method is sensitive to the presence of background emission and care should be taken to correct for any non-negligible background emission. In this work, we did not apply any scaling or normalization to the reference profiles, instead using the fluorescence intensities observed in the single-construct expressing cells directly.

A key goal of this work was to evaluate the extent of any uncertainty in the analysis. Fig. 3 visualizes the results of our analysis for cells expressing just one type of fluorophore. A visual inspection of example images indeed underscores a high degree of specificity within each of the detected channels (see Fig. 3A). To obtain statistically-relevant results, we performed an analysis on cells expressing single fluorophores (71 cells distributed over 31 field-of-views (FOVs) for Lyn-EGFP, 83 cells distributed over 39 FOVs for H2BffDronpa, 41 cells distributed over 22 FOVs for vimentin-ffDronpaF and 84 cells distributed over 40 FOVs for peroxisome-ffDronpa2F), by calculating the fluorescence brightness contribution determined for each fluorophore for the fourth (brightest) illumination pattern (see Equation (3) and Fig. 3B). These showed that on average about 80%–95% of the signal was correctly assigned by the analysis.

In order to estimate to what extent signals might be unaccounted for or spuriously generated by our analysis, we calculated a residual image for the fourth fluorescence image, showing the difference between the calculated and measured fluorescence intensities (this is equivalent to the refolded matrix  $\mathbf{E}$  – see Equation (1) and the Methods section). Fig. 3C visualizes these for the single-fluorophore data, showing that the magnitude of these residuals is within 10% of the calculated fluorescence brightnesses based on the comparison of the fluorescence intensity counts in the residual images in Fig. 3C with the counts in the images in Fig. 3A. A low amount of imperfectly captured structuring was observed in the residual images, particularly for ffDronpaF.

We sought to understand whether this imperfect separation could arise from the variability in the fluorophore response profiles observed between cells expressing the same construct, as was observed in Fig. 1D. To do so, we calculated fluorescence brightness contribution plots such

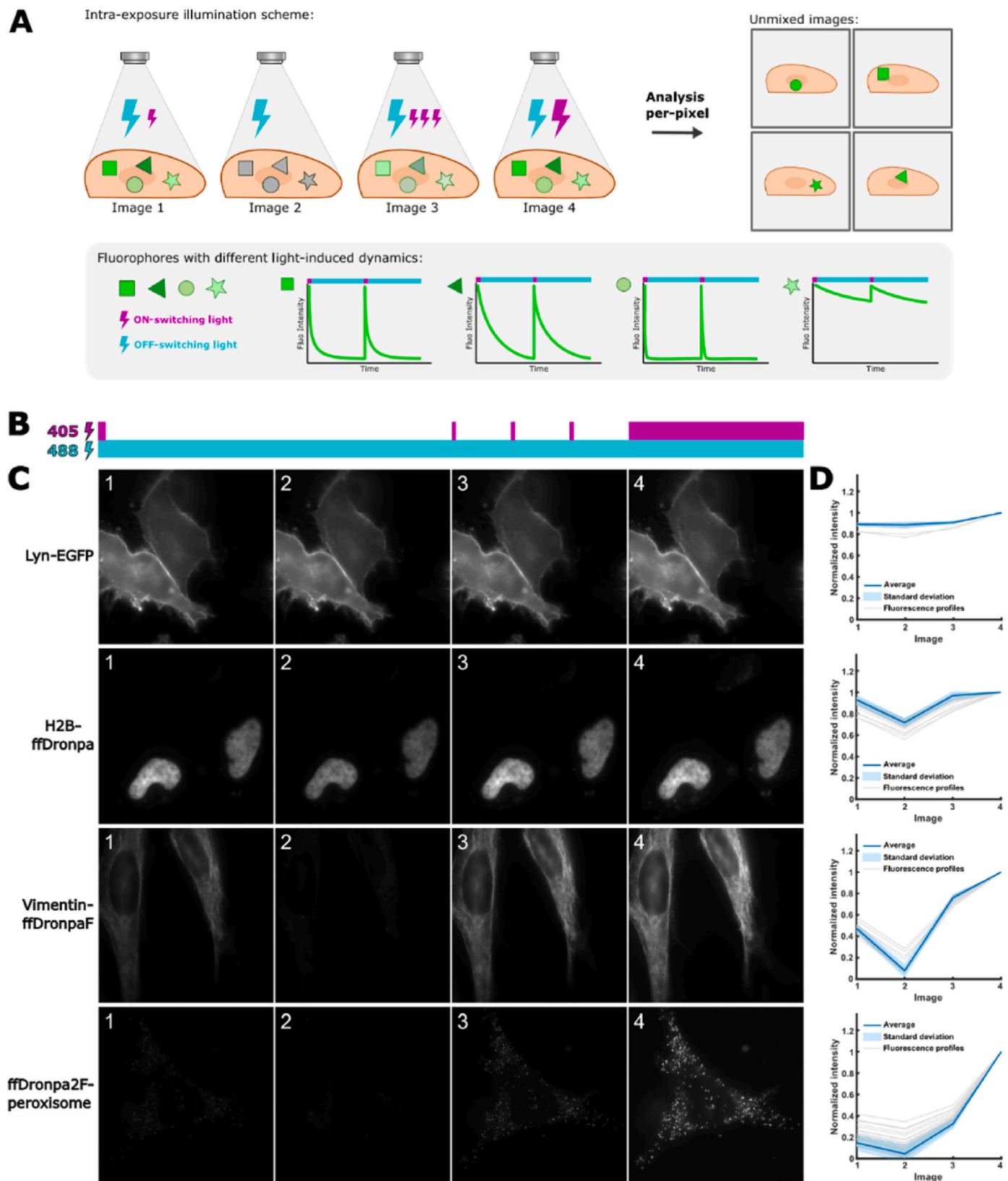


**Fig. 1.** A: Principle of the exNEEMO method. B: Illumination patterns used to probe the distinct photoswitching efficiencies and C: resulting fluorescence images for representative fixed HeLa cells that expressed a single fluorophore. D: Fluorescence profiles (normalized to the fourth image) for all cells expressing single fluorophores. Each line corresponds to a single distinct field-of-view (FOV). Scale bars 10  $\mu\text{m}$ .

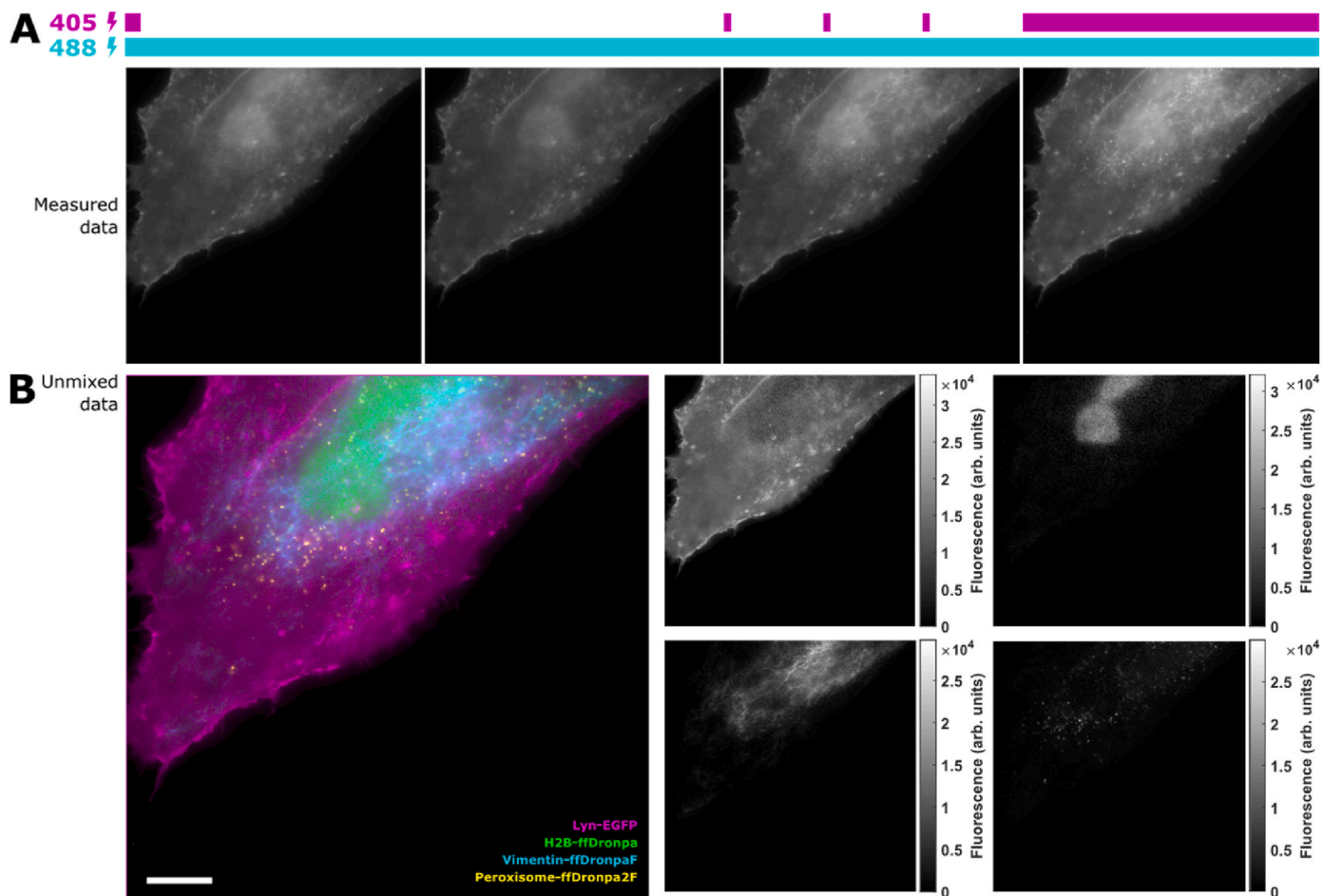


**Fig. 2.** A: HeLa cells expressing all four rsFPs imaged under the specific illumination scheme of violet and cyan light, resulting in a four-image sequence. B: False-color image showing the separation of the different emitter types using the exNEEMO analysis on the raw data shown in panel A. C: Distributions of the individual fluorophores for the same image as in panel B. Scale bars 10  $\mu$ m.

as those in Fig. 3B but each time varying the response profile of one fluorophore while keeping the remaining three response profiles constant. In other words, Equation (3) was applied repeatedly using one single rsFP response profile from an individual FOV and averaged response profiles for the other rsFPs considering all their respective FOVs. Fig. 4 shows an example for varying ffDronpa2F reference profiles, while Supplementary Fig. S3 shows this data also when varying the reference profiles of the other fluorophores. We find that the choice of reference profile has an effect on the extracted contributions, but the resulting variation is fairly small, apart from the contribution of specific FOVs that show clearly differing reference profiles (Supplementary Fig. S4). These deviating profiles were mainly associated with cells that were dimly fluorescent (Supplementary Fig. S5), that are intrinsically more difficult to analyze, and may also reflect variations induced by the fixation process [18]. These effects can be mitigated by performing a careful validation of the regions or cells selected as part of the single-fluorophore reference data. In practical applications of this method, we suggest the use of residual images such shown in Fig. 3C to identify situations where the measured signal cannot be adequately decomposed into the used reference profiles.

### 3. Conclusions

In this work, we have developed exNEEMO, an approach for the spatially-resolved separation of fluorophore mixtures based on their light-induced fluorescence dynamics. The core idea is to illuminate the sample with temporally-varying light intensities, to which the

fluorophores respond with characteristic emission profiles determined by the nature of the illumination pattern and the kinetics of their fluorescence dynamics. Compared to other approaches, our method has the advantage that it can make use of fluorescence dynamics that may occur too quickly to be resolved directly, but that are well within the rates at which even inexpensive light sources can be modulated. The exNEEMO experiments can in principle be carried out on any microscope that allows for the fast modulation of the excitation light. While we have here explored the method on fixed cells, our methodology should be directly applicable to live cell imaging as long as there is only little or no appreciable change in the cell structuring during the acquisition of the four fluorescence images.

Compared to our previous work, which was focused on the classification of samples expressing a single fluorophore each, the methodology in this work can resolve fluorophore mixtures down to the 'per-pixel' limit in which the full spatial resolution of the imaging is retained. To do so, we assume that the characteristic fluorophore response profiles are known in advance or can be obtained through measurements of samples expressing a single fluorophore. We analyzed the experimental data using non-negative least squares, which decomposes the measured signal into a weighted sum of the individual fluorophore reference profiles. This analysis does not take into account that the local fluorophore environment or illumination conditions may cause deviations of the reference profiles, which can lead to artifacts in the analysis. Fully addressing such issues will require the development of analysis algorithms that can dynamically adjust the reference profiles to account for changes in probe behavior that may arise within particular (cellular)



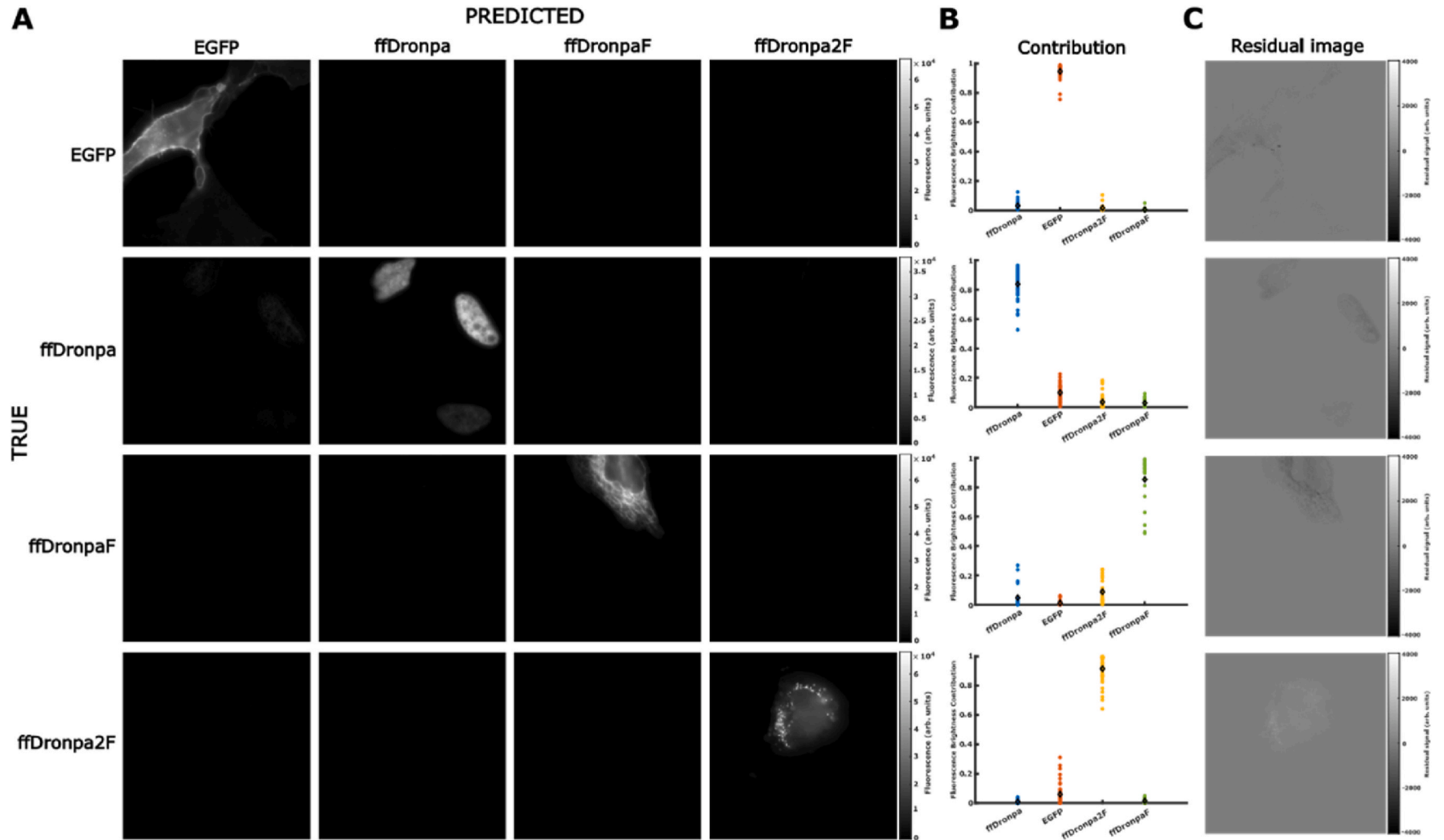


**Fig. 3.** A: exNEEMO analysis of the cells expressing a single rsFP. B: Unmixing accuracies of each rsFP shown as fluorescence brightness contribution plots. One dot represents one FOV. The diamond represents the average. C: Images showing the residual signal when subtracting the fourth image produced by the exNEEMO from the fourth measured fluorescence image. Contributions of all four components were used in the calculation of the residual images.

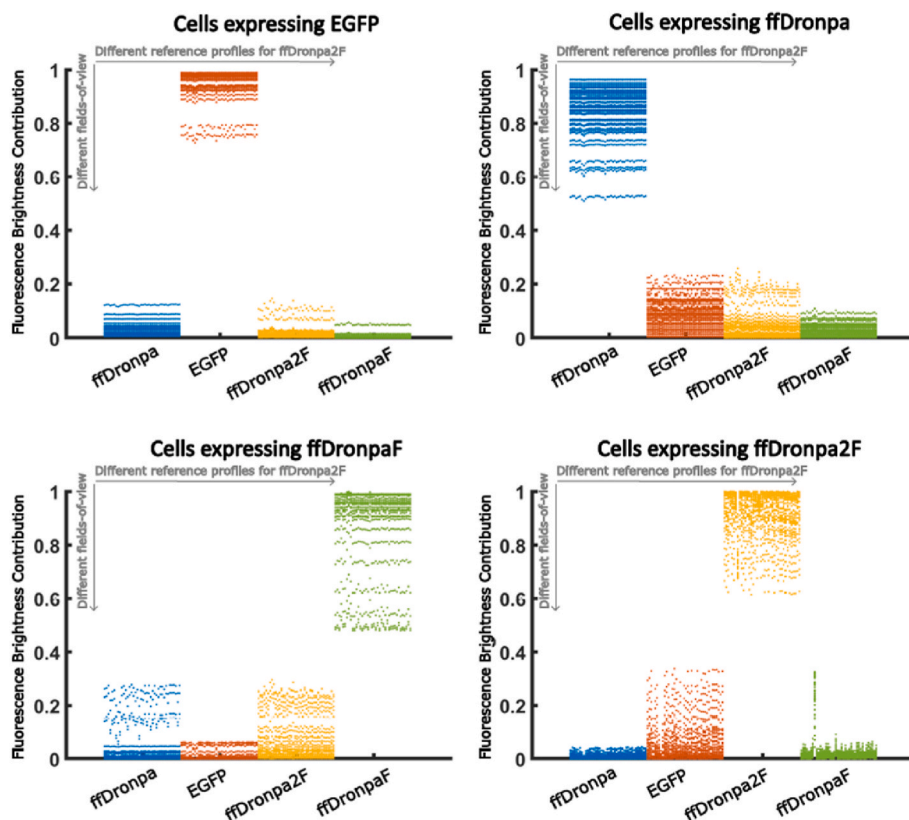


**Fig. 4.** Influence of the reference profile on the fluorophore contribution in the exNEEMO output. Example of a contribution plot showing fluorescence brightness contributions of each rsFP in the single-fluorophore datasets, where reference profiles of ffDronpa2F are varied. Data points along the y-axis denote different FOVs. A selection showing individual reference profiles and their unmixing results can be found in [Supplementary Fig. S4](#).

environments. Such algorithms may well be guided by minimizing the structuring observed in the residual images in order to deliver an emitter separation that accounts for the full measured signal.

Our approach complements the currently-available methods to discriminate spectrally-overlapping probes in a spatially-resolved manner. Compared to fluorescence lifetime imaging (FLIM), for example, our approach holds the advantage that it has much lower instrumental requirements and allows the use of more sensitive cameras, but the disadvantages that it can only be applied to a limited range of fluorophores and in contexts where the light-induced fluorophore responses can be predicted based on reference measurements. In principle, both methodologies could also be combined in order to increase the number of labels that can be distinguished.

In conclusion, using exNEEMO we were able to distinguish four green rsFPs in eukaryotic cells in a per-pixel manner that maintains the full spatial resolution of the imaging. Technically, the principle of exNEEMO can be transferred to photochromic probes of other colors, which would only require wavelength adjustment of the illumination sequence. Similarly to our previous work, the key advantage of the method is the ability to operate on a wide range of fluorescence dynamics since it is not limited by the temporal resolution of the detector. By providing increased multiplexing opportunities using a conceptually simple approach, our method opens new dimensions for high-content imaging in complex (biological) systems.

#### CRediT author statement

**Hana Valenta:** Investigation, Formal Analysis, Writing - Original Draft, Writing - Review & Editing, Visualization, **Franziska Bierbuesse:** Software, Formal Analysis, Investigation, Writing - Original Draft, Writing - Review & Editing, Visualization, **Raffaele Vitale:** Software, Writing - Review & Editing, **Cyril Ruckebusch:** Writing - Review &

Editing, **Wim Vandenberg:** Conceptualization, **Peter Dedecker:** Conceptualization, Writing - Original Draft, Writing - Review & Editing, Supervision, Funding Acquisition.

#### Methods

##### Plasmids

As in our previous work [8], the fluorophores used in this project were EGFP, ffDronpa, ffDronpaF (ffDronpaK45I/F173V), and ffDronpa2F (ffDronpa K45I/M159 T/F173V). Plasmids coding for expression of these fluorophores in mammalian cells, *i.e.*, pcDNA3-Lyn11-EGFP (with N-terminal MGC1KSKGKDSAGGGS targeting sequence), pH2B-ffDronpa (targeted to the histone H2B in the nucleus), pVimentin-ffDronpaF (targeted to the vimentin in the cell cytoskeleton), were already available in the lab. A plasmid for ffDronpa2F targeted to the peroxisome was generated by replacing EGFP with ffDronpa2F with C-terminal SKL sequence in the pEGFP-N1 vector.

##### Mammalian cell culture, transfection and fixation

HeLa cells were grown at 37 °C in 5 % CO<sub>2</sub> atmosphere in DMEM (ThermoFisher) with GlutaMAX-1 complemented with 10 % fetal bovine serum (FBS) and GlutaMAX (ThermoFisher). Cells were seeded in 35-mm glass-bottom dishes (MatTek) and after 24 h they were transiently transfected using X-tremeGENE HP DNA Transfection Reagent (Roche) according to the manufacturer's protocol. 24 h after the transfection, cells were washed with 1 × Dulbecco's phosphate-buffered saline (DPBS), pre-fixed with 4 % paraformaldehyde (PFA, Electron Microscopy Sciences) solution for 2 min at RT, washed with 1 × DPBS and then the fixation was completed with 4 % PFA for 12 min at RT. The pre-fixation step helps to preserve the native protein structures in the cells.

Afterwards, cells were incubated with 10 % glycine for 10 min at RT and then washed four times with  $1 \times$  DPBS. Dishes with fixed cells were stored in  $4^\circ\text{C}$  in  $1 \times$  DPBS in the dark until the imaging experiment.

### Widefield image acquisition

Imaging of the fixed cells was performed on a Nikon Eclipse Ti-2 Inverted Microscope (Minato City, Japan) equipped with a 1.4 NA oil immersion objective ( $100 \times$  CFI Apochromat Total Internal Reflection Fluorescence) and a ZT405/488/561/640rpcv2 dichroic mirror with a ZET405/488/561/640 nm emission filter (both Chroma Technology, Bellows Falls, Vermont) in epi-illumination. Two separate lasers at 405 and 488 nm (Oxxius, Lannion, France) were used for excitation. Images were acquired on a PCO. edge 4.2 camera (PCO, Kelheim, Germany) with an exposure time of 50 ms and an optical pixel size of 78.8 nm, using varying pulses of the 405 nm light ( $37.5 \text{ W/cm}^2$ ) in the presence of 488 nm light ( $29.5 \text{ W/cm}^2$ ). The excitation light was controlled using an Arduino-compatible microcontroller (Velleman, Gavere, Belgium). The duration of the pulses within the four images was the same as in Ref. [8] and is shown in [Supplementary Table S1](#). To avoid any issues with deviating initial photoswitching behavior occasionally observed in some fluorescent probes [19], we consecutively acquired two sets of four modulated images and used the last set in the analysis and characterization. Due to the rolling-shutter readout process, the 50 ms camera exposure resulted in a maximal per-image illumination duration of 40 ms since light was applied only when all of the camera pixels were sensitive. To increase the total number of images, the acquisition was performed at equidistant positions over a whole dish using an automated stage loop. FOVs that were out of focus, contained emission that saturated the camera, did not contain any cells or contained clearly degraded cells were excluded from the image analysis.

### Image analysis

The image analysis was carried out by means of non-negative least squares. As was described in the text above (see also [16,17]), we solve under a non-negativity constraint

$$\mathbf{X} = \mathbf{A}\mathbf{S}^T + \mathbf{E} \quad (2)$$

for the matrix  $\mathbf{A}$  that denotes the abundance of each fluorophore in every camera pixel, given the measured image  $\mathbf{X}$ , the matrix  $\mathbf{S}$  that contains the reference profiles and  $\mathbf{E}$  an error or residual matrix that describes to what extent the calculated solution deviates from the measured values. In our experiments,  $\mathbf{X}$ ,  $\mathbf{A}$ , and  $\mathbf{E}$  are of dimensions  $N \times 4$ , where  $N$  is the total number of pixels in a fluorescence image and 4 is the number of images. To fill  $\mathbf{X}$ , the four images acquired with different illumination patterns are simply unfolded by concatenating all of the pixel values from a given image into a column of  $\mathbf{X}$ . The matrix  $\mathbf{S}$  is a  $4 \times 4$  matrix containing the responses of the fluorophores as determined from the single-fluorophore control measurements. The dimensions of this matrix arise because we have four different fluorophores and four different illumination patterns. The actual algorithm used to solve this equation is described in Ref. [15] and given in the toolbox [20].

To reduce the influence of background areas on the analysis, we segmented the acquired images by calculating an average of the four images and determining a threshold value  $T = (\max - \min) \cdot 0.05 + \min$ , where ‘max’ and ‘min’ refer to the intensities of the brightest and dimmest pixels in this average image. Pixels with intensities smaller than  $T$  were deemed to correspond to the background signal and removed from the analysis, resulting in the exclusion of an identical set of pixels from all four of the acquired images. To correct for the contribution of the background signal, we calculated the average signal associated with the excluded pixels in each of the four images, subtracting this from the corresponding images. These background-corrected images were then analyzed as described in the preceding paragraph.

To determine the components of the matrix  $\mathbf{S}$ , the four images acquired in cells expressing a single fluorophore construct were first segmented and background-corrected as described above. The single-fluorophore reference profiles were then extracted by calculating the average fluorescence intensities observed in each measured image in the FOV for the pixels above the threshold. The final reference profiles used in matrix  $\mathbf{S}$  are determined by averaging the profiles of all acquired FOVs for the respective fluorophore. These reference profiles were used without further normalization.

The contribution graphs in [Fig. 3B](#) and elsewhere show the averaged fractional contribution of each fluorophore calculated for the single-fluorophore reference data. To calculate the fractional contribution  $c_k$  of the  $k$ -th fluorophore to the fourth (brightest) measured frame, we make use of

$$c_k = \frac{\sum_{l=1}^N a_{lk} s_{k4}}{\sum_{m=1}^N \left( \sum_{l=1}^4 a_{ml} s_{l4} \right)} \quad (3)$$

where the indices  $l$  and  $k$  refer to the fluorophores ffDronpa, EGFP, ffDronpa2F and ffDronpaF. The summation indices  $l$  and  $m$  run over a  $N$  image pixels included in the analysis. The contribution  $c_k$  is calculated independently for each FOV, leading to the individual datapoints shown in [Fig. 3B](#). For the contribution graphs with varied reference profiles, we changed the reference profile for one fluorophore and used the average profiles for the other three fluorophores. The varied profiles were extracted from the individual single-fluorophore FOVs. The homemade analysis routine was written for MATLAB R2022a (The MathWorks, Natick, MA). The full source code and experimental data are available online at [21].

### Declaration of competing interest

The authors declare that they have no known competing financial interests or personal relationships that could have appeared to influence the work reported in this paper.

### Data availability

The full source code, written for MATLAB R2022a (The MathWorks, Natick, MA), and experimental data are available online at <https://doi.org/10.5281/zenodo.10078873>.

### Acknowledgements

This work was supported by the Research Foundation-Flanders (FWO) via grants G010723N and G090819N, FLAG-ERA via grant JTC2019 Sensei, and the University of Lille via their International Chair program.

### Appendix A. Supplementary data

Supplementary data to this article can be found online at <https://doi.org/10.1016/j.talanta.2023.125397>.

### References

- [1] Junyoung Seo, Yeonbo Sim, Jeewon Kim, Hyunwoo Kim, In Cho, Hoyeon Nam, Young-Gyu Yoon, Jae-Byum Chang, PICASSO allows ultra-multiplexed fluorescence imaging of spatially overlapping proteins without reference spectra measurements, *Nat. Commun.* 13 (1) (May 2022) 2475.
- [2] Ilaria Testa, Andreas Schönle, Claas v. Middendorff, Claudia Geisler, Rebecca Medda, Christian A. Wurm, Andre C. Stiel, Stefan Jakobs, Mariano Bossi, Christian Eggeling, Stefan W. Hell, Egnor Alexander, Nanoscale separation of molecular species based on their rotational mobility, *Opt Express* 16 (25) (Dec 2008) 21093–21104, <https://doi.org/10.1364/OE.16.021093>. URL, <http://opg.optica.org/oe/abstract.cfm?URI=oe-16-25-21093>.
- [3] Thomas Niehörster, Anna Löscherberger, Ingo Gregor, Benedikt Krämer, Hans-Jürgen Rahn, Matthias Patting, Felix Koberling, Jörg Enderlein, Markus Sauer,



- Multi-target spectrally resolved fluorescence lifetime imaging microscopy, *Nat. Methods* 13 (3) (Mar 2016) 257–262, <https://doi.org/10.1038/nmeth.3740>.
- [4] Gerard Marriott, Shu Mao, Tomoyo Sakata, Ran Jing, David K. Jackson, Chutima Petchprayoon, Timothy J. Gomez, Erica Warp, Orapim Tulyathan, Holly L. Aaron, Ehud Y. Isacoff, Yuling Yan, Optical lockin detection imaging microscopy for contrast-enhanced imaging in living cells, *Proc. Natl. Acad. Sci. USA* 105 (46) (2008) 17789–17794, <https://doi.org/10.1073/pnas.0808882105>. <https://www.pnas.org/content/105/46/17789>.
- [5] Jérôme Querard, Tal-Zvi Markus, Marie-Aude Plamont, Carole Gauron, Pengcheng Wang, Agathe Espagne, Michel Volovitch, Sophie Vriz, Vincent Croquette, Arnaud Gautier, Thomas Le Saux, Ludovic Jullien, Photoswitching kinetics and phase-sensitive detection add discriminative dimensions for selective fluorescence imaging, *Angew. Chem. Int. Ed.* 54 (9) (2015) 2633–2637, <https://doi.org/10.1002/anie.201408985>. <https://onlinelibrary.wiley.com/doi/abs/10.1002/anie.201408985>.
- [6] Sam Duwé, Wim Vandenberg, Peter Dedecker, Live-cell monochromatic dual-label sub-diffraction microscopy by mt-pcSOFI, *Chem. Commun.* 53 (2017) 7242–7245, <https://doi.org/10.1039/C7CC02344H>.
- [7] Daniel Wüstner, Dynamic mode decomposition of fluorescence loss in photobleaching microscopy data for model-free analysis of protein transport and aggregation in living cells, *Sensors* 22 (13) (2022) 4731, <https://doi.org/10.3390/s22134731>.
- [8] Hana Valenta, Siewert Hugelier, Duwé Sam, Giulia Lo Gerfo, Marcel Müller, Peter Dedecker, Wim Vandenberg, Separation of spectrally overlapping fluorophores using intra-exposure excitation modulation, *Biophysical Reports* 1 (2) (Dec 2021), 100026. <https://www.sciencedirect.com/science/article/pii/S2667074721000264>.
- [9] Chouket Raja, Agnès Pellissier-Tanon, Aliénor Lahlou, Ruikang Zhang, Diana Kim, Marie-Aude Plamont, Mingshu Zhang, Xi Zhang, Pingyong Xu, Nicolas Desprat, Dominique Bourgeois, Agathe Espagne, Annie Lemarchand, Thomas Le Saux, Ludovic Jullien, Extra kinetic dimensions for label discrimination., *Nat. Commun.* 13 (1) (Mar 2022) 1482, <https://doi.org/10.1038/s41467-022-29172-0>.
- [10] Yuling Yan, M Emma Marriott, Chutima Petchprayoon, Gerard Marriott, Optical switch probes and optical lock-in detection (OLID) imaging microscopy: high-contrast fluorescence imaging within living systems, *Biochem. J.* 433 (3) (Feb 2011) 411–422, <https://doi.org/10.1042/BJ20100992>.
- [11] Jung-Cheng Hsiang, Amy E. Jablonski, Robert M. Dickson, Optically modulated fluorescence bioimaging: visualizing obscured fluorophores in high background, *Acc. Chem. Res.* 47 (5) (May 2014) 1545–1554, <https://doi.org/10.1021/ar400325y>.
- [12] Gerardo Abbandonato, Barbara Storti, Giovanni Signore, Fabio Beltram, Ranieri Bizzarri, Quantitative optical lock-in detection for quantitative imaging of switchable and non-switchable components, *Microsc. Res. Tech.* 79 (10) (Oct 2016) 929–937, <https://doi.org/10.1002/jemt.22724>.
- [13] Jérôme Querard, Ruikang Zhang, Zsolt Kelemen, Marie-Aude Plamont, Xiaojiang Xie, Chouket Raja, Insa Roemgens, Yulia Korepina, Samantha Albright, Eliane Ipendey, Michel Volovitch, Hanna L. Sladitschek, Neveu Pierre, Lionel Gissot, Arnaud Gautier, Jean-Denis Faure, Vincent Croquette, Thomas Le Saux, and Ludovic Jullien. Resonant out-of-phase fluorescence microscopy and remote imaging overcome spectral limitations, *Nat. Commun.* 8 (1) (2017) 969.
- [14] Agnès Pellissier-Tanon, Chouket Raja, Ruikang Zhang, Aliénor Lahlou, Agathe Espagne, Annie Lemarchand, Vincent Croquette, Ludovic Jullien, Thomas Le Saux, Resonances at fundamental and harmonic frequencies for selective imaging of sine-wave illuminated reversibly photoactivatable labels, *ChemPhysChem* 23 (23) (2022), e202200295, <https://doi.org/10.1002/cphc.202200295>.
- [15] Rasmus Bro, Sijmen De Jong, A fast non-negativity-constrained least squares algorithm, *J. Chemometr.* 11 (5) (1997) 393–401.
- [16] Cyril Ruckebusch, Beata Walczak, Lutgarde Buydens, *Resolving Spectral Mixtures with Applications from Ultrafast Time-Resolved Spectroscopy to Super-resolution Imaging. Data Handling in Science and Technology*, Elsevier, 2016.
- [17] Siewert Hugelier, Raffaele Vitale, Cyril Ruckebusch, 4.17 - image processing in chemometrics, Oxford, second edition edition, in: Steven Brown, Romà Tauler, Beata Walczak (Eds.), *Comprehensive Chemometrics*, second ed., Elsevier, 2020, pp. 411–436, <https://doi.org/10.1016/B978-0-12-409547-2.14597-4>. ISBN 978-0-444-64166-3, <https://www.sciencedirect.com/science/article/pii/B9780124095472145974>.
- [18] Katharina N. Richter, Natalia H. Revelo, Katharina J. Seitz, Martin S. Helm, Deblina Sarkar, Rebecca S. Saleeb, Elisa D'Este, Jessica Eberle, Eva Wagner, Christian Vogl, Diana F. Lazaro, Frank Richter, Javier Coy-Vergara, Giovanna Coceano, Edward S. Boyden, Rory R. Duncan, Stefan W. Hell, Marcel A. Lauterbach, Stephan E. Lehnart, Tobias Moser, Tiago F. Outeiro, Rehling Peter, Blanche Schwappach, Ilaria Testa, Bolek Zapiec, Silvio O. Rizzoli, Glyoxal as an alternative fixative to formaldehyde in immunostaining and super-resolution microscopy, *EMBO J.* 37 (1) (2018) 139–159, <https://doi.org/10.15252/emboj.201695709>.
- [19] Anaïs C. Bourges, Benjamien Moeyaert, Thi Yen Hang Bui, Franziska Bierbuesse, Wim Vandenberg, Peter Dedecker, Quantitative determination of the full switching cycle of photochromic fluorescent proteins, *Chem. Commun.* 59 (2023) 8810–8813, <https://doi.org/10.1039/D3CC01617J>.
- [20] Joaquim Jaumot, Romà Tauler, Anna de Juan, MCR-ALS 2.0 Toolbox, URL, March 2022, <https://doi.org/10.5281/zenodo.6334791>.
- [21] Quantitative determination of the full switching cycle of photochromic fluorescent proteins, *bioRxiv*. (November 2023). <https://doi.org/10.5281/zenodo.10078873>.